



Enhancing charge density and steering charge unidirectional flow in 2D non-metallic semiconductor-CNTs-metal coupled photocatalyst for solar energy conversion

Xiaojie She^a, Jingjie Wu^b, Hui Xu^{a,b,*}, Zhao Mo^a, Jiabiao Lian^a, Yanhua Song^{b,c}, Liang Liu^a, Daolin Du^a, Huaming Li^{a,**}

^a School of the Environment and Safety Engineering, Institute for Energy Research, Jiangsu University, Zhenjiang 212013, PR China

^b Department of Materials Science and NanoEngineering, Rice University, Houston, TX 77005, USA

^c School of Environmental and Chemical Engineering, Jiangsu University of Science and Technology, Zhenjiang 212003, PR China

ARTICLE INFO

Article history:

Received 7 July 2016

Received in revised form 30 August 2016

Accepted 4 September 2016

Available online 5 September 2016

Keywords:

Steering electron unidirectional flow

Photocatalysis

H₂ evolution

ABSTRACT

The effective separation of the electron and hole (e-h) pairs plays a key role in enhancing the photocatalytic performance of the semiconductors. The density of electrons participating in the reduction reaction also determines photocatalytic performance. We report here a rational design of a photocatalyst assembly composed of n-type semiconducting two-dimensional g-C₃N₄ nanosheets (2D-C₃N₄), carbon nanotubes (CNTs), and plasmonic Ag nanocubes, which exhibits enhanced density of electrons and controlled unidirectional charge flow to promote the photocatalytic hydrogen evolution reaction. Plasmonic Ag nanocubes inject the hot-electrons into conduction band of 2D-C₃N₄ to increase the density of electrons while the CNTs act as a power pump of the electrons to steer electron flow from the conduction band of 2D-C₃N₄ to reactants. The photocatalytic performance of Ag/2D-C₃N₄/CNTs assembly was dramatically enhanced for the H₂ evolution from water. The enhanced photocatalytic activity is due to the efficient unidirectional transfer of the electrons with high density and efficient separation of the e-h pairs.

© 2016 Elsevier B.V. All rights reserved.

1. Introduction

The photocatalysis, as one of the most perspective technologies for clean energy conversion and environmental protection, involves semiconductors to absorb light to induce photoexcited electrons and holes to participate in redox reaction [1–3]. Aside the electrons/holes transporting to the semiconductor surface and then being received by reaction molecules, the electrons and holes (e-h) tend to recombine resulted in reducing of the photocatalytic activity [4]. Therefore, it's essential to suppress (e-h) recombination to improve the photocatalyst performance [5]. For example, some conductive materials (e.g. graphene and carbon nanotubes) as the power pump of the charge carriers, are often used as electron acceptor to improve the efficiency of e-h separation [6–9]. On the other hand, the redox capability of the photocatalyst is determined by the edge positions of its valence band (VB) and conduction band (CB) [5]. More positive energy of VB or more negative energy of CB

possesses stronger oxidation or reduction capability, signifying that a wider bandgap is more active due to the higher redox ability [5]. However, the wide bandgap photocatalyst only absorbs the ultraviolet light that accounts for ~4% of incoming solar energy [10–12]. Obviously, it cannot meet the needs of the practical application. So far, the bandgap of the photocatalyst has been usually restricted to enable photocatalyst absorbing visible light (>400 nm). In addition, to further enhance the photocatalytic performance and improve utilization of the visible light, the surface plasmon of the metals has been usually introduced into semiconductor. For example, the metals (Cu, Ag, Au, etc) with the surface plasmonic effect loaded on the surface of the semiconductors can absorb visible light, and then produce and inject the hot charge carriers into the semiconductor, which can improve the density of the charge carriers of the semiconductor and sequentially improve photocatalytic activity [13–17].

For the past few years, as an n-type semiconductor, the graphitic carbon nitride (g-C₃N₄) has gained a lot of attention due to the nonmetallic and nontoxic nature, and high thermal and chemical stability [18–20]. Note that this material doesn't possess the stoichiometric ratio of C₃N₄, it also contains some hydrogen elements. In order to keep consistency with the previous literatures, the term "graphitic carbon nitride" ("g-C₃N₄") are still used in this

* Corresponding author at: School of the Environment and Safety Engineering, Institute for Energy Research, Jiangsu University, Zhenjiang 212013, PR China

** Corresponding author.

E-mail addresses: xh@ujs.edu.cn (H. Xu), lihm@ujs.edu.cn (H. Li).

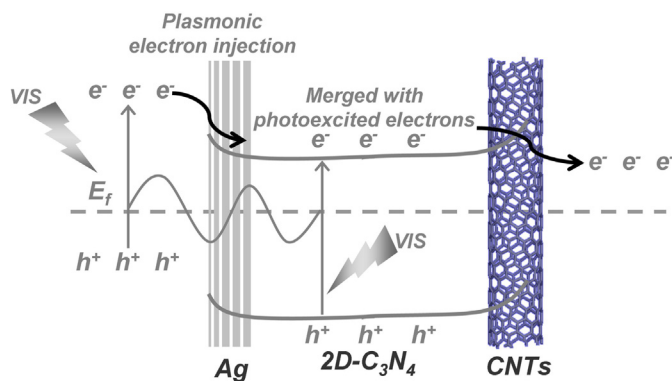


Fig. 1. Schematic illustration of the band alignment and electrons flow in the designed composite photocatalyst.

work. The g-C₃N₄ with appropriate CB and VB has been widely applied in H₂ evolution from the water, photocatalytic organic pollution degradation and photocatalytic CO₂ reduction under the visible light irradiation [10,20]. However, the bulk g-C₃N₄ is not a promising photocatalyst due to many disadvantages, such as the high e-h recombination rate, low specific surface area, and weak redox ability [5,21–23]. Thus, many strategies have been used to overcome these drawbacks, such as through morphology control, introduction of Schottky junction by metals, preparation of the composites [24–27]. Therein, two-dimension or few-layer g-C₃N₄ nanosheets (2D-C₃N₄) show the attractive properties [18,25,28,29]. 2D structure not only improves efficiency of e-h separation, but also enlarges the bandgap of the g-C₃N₄ (enhance redox ability) [25,28]. However, the photocatalytic efficiency of the pure 2D-C₃N₄ is still deficient in the absence of the other co-catalysts or semiconductors [28,29]. The major reason lies in (1) short of the driving force to unidirectionally steer the electron transport and (2) low density of the electrons at CB of 2D-C₃N₄ [5].

In this work, we developed a strategy to steer flow of charge carriers with an enhanced density to improve photocatalytic activity of the semiconducting photocatalyst. In the designed composite photocatalyst, the hot electrons injected by plasmonic metals can flow to CB of the semiconductor and merge with the photogenerated electrons of the semiconductor under the visible light irradiation. Subsequently these high density electrons continue streaming unidirectionally to the excellent electrical conductor to participate in reduction reaction, as shown in Fig. 1. As a proof of concept, we chose 2D-C₃N₄ as a base semiconducting photocatalyst modified with the carbon nanotubes (CNTs) as electron acceptor (the power pump of the electrons) and the noble metal Ag as electron donor. 2D-C₃N₄ possesses the wider bandgap (the stronger redox ability) with comparison to the bulk g-C₃N₄. CNTs is cheaper compared with the other conductive materials and has the excellent electrical conductivity while the surface plasmon of Ag is stable in the range of the visible light.

2. Materials and experimental procedure

2.1. Chemicals

Melamine (>99% purity), Ethylene glycol (EG) (>99.0%), Acetone (>99.5%), Ethanol (99.7%), were purchased from Sinopharm Chemical Reagent Co., Ltd. (China). Multiwalled carbon nanotube (CNTs, >95%) was purchased from Chengdu Organic Chemicals Co., Ltd., Chinese Academy of Sciences. Poly(vinyl pyrrolidone) (PVP, Mw = ~55000) and Sodium hydrosulfide (NaSH) were purchased from Sigma Aldrich. Silver trifluoroacetate (CF₃COOAg) was purchased from Aladdin. Doubly distilled water was used in our

experiments. All chemicals were of analytical reagent grade and used as received without further purification.

2.2. Synthesis of the samples

The bulk g-C₃N₄ was prepared by the thermal polycondensation method. In a typical synthesis, 2 g melamine was heated at 550 °C for 4 h with 2 °C/min in a crucible with a cover [10]. After that, the yellow sample was ground into the powder for further use. CNTs/g-C₃N₄ was synthesized by the same method as that of preparing the bulk g-C₃N₄, except mixing CNTs with precursor in advance. In a typical synthesis, the CNTs was dispersed in water to form a 0.1 mg/mL CNTs aqueous suspension by the sonication for 1 h. 5 mL CNTs aqueous suspension was added into 2 g melamine in a crucible. Subsequently, the suspension was stirred for 30 min under magnetic stirrers. The heating program was the same as that of preparing the bulk g-C₃N₄. The color of CNTs/g-C₃N₄ was dingy yellow.

The CNTs/2D-C₃N₄ was prepared by heating CNTs/g-C₃N₄ for a second time. In a typical procedure, 400 mg CNTs/g-C₃N₄ in the porcelain boat was heated at 550 °C for ~110 min. After that, the as-obtained product is gray. In the CNTs/2D-C₃N₄ composite, the semiconductor (g-C₃N₄) has few-layer nanosheet structure, thus, it is denoted as 2D-C₃N₄. For Ag/2D-C₃N₄/CNTs, 10 mg CNTs/g-C₃N₄ was dispersed in 10 mL H₂O through sonication. Then 0.4 mL of Ag nanocubes aqueous solution (0.5 mg/mL) was added into the suspension (the preparation of Ag nanocubes is in Supporting information). The mixture was sonicated for 30 min and stirred for another 30 min. And then the mixture was transferred to a Teflon-lined stainless steel autoclave with a 20 mL capacity and heated at 120 °C for 1 h. The final product was separated by centrifugation and washed with water several times. Then the final sample was freeze-dried for 24 h.

2.3. Photoelectrochemical measurement

The samples were dispersed in 50% ethanol and 50% EG through sonication and the concentration of the suspension was 1 mg/mL. Then, 20 μL of the suspension was drop-casted onto an indium tin oxide (ITO)-coated glass with an exposed area of 0.5 cm² (1 cm × 0.5 cm), and dried under the infrared lamp irradiation (unless otherwise noted, the electrodes were prepared by the above method). In the experiment, all sample-modified ITO electrodes were prepared via the above method unless otherwise specified. The CHI660B electrochemical analyzer was used. All photocurrent measurements were performed under a standard three-electrode system, with a platinum wire used as the counter electrode, indium tin oxide (ITO) glass as the working electrode and Ag/AgCl (saturated KCl solution) as the reference electrode. A bias potential of –0.2 V (vs. Ag/AgCl) was used in the experiments. Sodium sulfate solution (Na₂SO₄, 0.1 M) was used as the electrolyte. Unless otherwise noted, a 500 W Xe lamp was employed as the light source.

2.4. Photocatalytic activity

For photocatalytic hydrogen production reaction, triethanolamine was used to sacrifice the holes. 10 mg of photocatalysts were dispersed in 100 mL triethanolamine/H₂O (10% triethanolamine). Then, the co-catalyst Pt was in-situ photodeposited on the surface of photocatalysts by adding H₂PtCl₆. The suspension was sonicated to make the suspension uniform. Before visible-light irradiation, the suspension was fully degassed to remove air. A 300 W Xenon lamp (PLS-SXE 300C (BF), Perfect-Light, Beijing) with an optical filter ($\lambda > 400$ nm) was used as the visible-light source. The measured incident power of light was ~0.246 W·cm⁻². The diameter of the window of the lamp source

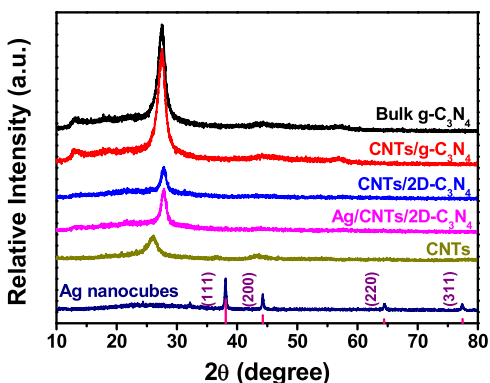


Fig. 2. XRD patterns of the CNTs, Ag nanocubes, bulk g-C₃N₄, CNTs/g-C₃N₄, CNTs/2D-C₃N₄ and Ag/2D-C₃N₄/CNTs.

is 4.8 cm. The amount of H₂ evolved was quantified by the gas chromatograph (GC D7900P, TCD detector, N₂ carrier gas, 5A molecular sieve column, Shanghai Fechcomp).

3. Results and discussion

The crystal structures of all photocatalysts were firstly characterized by the powder X-ray diffraction (XRD), as shown in Fig. 2. The XRD peak of CNTs at ~26.2° is attributed to its (002) crystal plane, indicating that CNTs have a high crystallinity [30]. The XRD peaks of Ag nanocubes at ~38.1°, 44.3°, 64.4° and 77.5° are attributed to its (111), (200), (220) and (311) crystal plane (JCPDS 87-0597), respectively. For the composites, the corresponding XRD peaks of Ag and CNTs don't emerge, which is ascribed to the low content of Ag and CNTs in composite. The samples including bulk g-C₃N₄ shows peaks at ~13.1° (100) and 27.7° (002) ascribed to the in-plane repeated units and interlayer stacking reflections of g-C₃N₄, respectively [10,31]. In the 2D-C₃N₄ based composite photocatalysts, no (100) peak is observable because of 2D structural nature [18,25,29]. Obviously, from XRD results, the crystal structure of 2D-C₃N₄ in composites remain intact.

The morphologies of all samples were characterized via the transmission electron microscope (TEM) and the field emission scanning electron microscope (FE-SEM). Fig. S1a and c is the FE-SEM and TEM images of CNTs displaying an average diameter (~20 nm) and length (~1 μm), respectively. The high-magnification FE-SEM and low-magnification TEM images show homogeneous size (~50 nm) of Ag nanocubes (Fig. S1b and d). CNTs/2D-C₃N₄ and Ag/2D-C₃N₄/CNTs display nanosheet morphology (Fig. S1g and h). And after a long ultrasonication treatment, for Ag/2D-C₃N₄/CNTs composite, Ag nanocubes did not separate from the face of CNTs/2D-C₃N₄, as shown in Fig. S1i and j. Additionally, under the same scale, for the mixture of Ag nanocubes and CNTs/2D-C₃N₄, it is obviously that many Ag nanocubes scattered on the side of the substrate. However, for Ag/2D-C₃N₄/CNTs composite, Ag nanocubes did not separate from CNTs/2D-C₃N₄, as shown in Fig. S1k and l. These indicates that Ag nanocubes and CNTs/2D-C₃N₄ can bond together well by the hydrothermal method. CNTs were occasionally found in TEM image of CNTs/2D-C₃N₄ composite (Fig. 3a). The TEM image of Ag/2D-C₃N₄/CNTs shows that a small percent of CNTs and Ag nanocubes are anchored onto the ultrathin 2D-C₃N₄ (Fig. 3b). In addition, the bulk g-C₃N₄ and CNTs/g-C₃N₄ look like solid rocks, as shown in Fig. S1e and f. In CNTs/g-C₃N₄ composite, it is difficult to find CNTs because of the trace content of CNTs.

The FT-IR spectra of all samples are similar to each other and correspond to the chemical structure of g-C₃N₄ (Fig. S2). The peak at ~810 cm⁻¹ is attributed to the breathing mode of the s-triazine ring [10]. The peaks between ~1800 to 900 cm⁻¹ are assigned to the

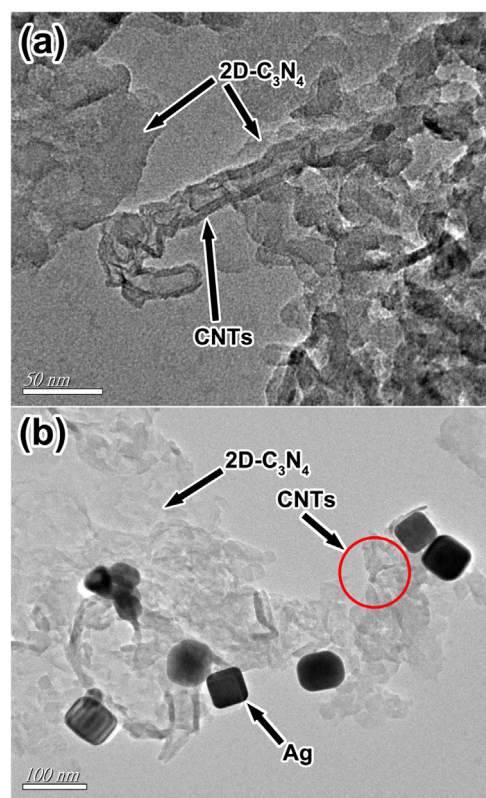


Fig. 3. The TEM images of (a) CNTs/2D-C₃N₄ and (b) Ag/2D-C₃N₄/CNTs.

stretching vibration of C=N and C–N heterocycles [29]. The broad ones from ~3600–3000 cm⁻¹ are attributed to the N–H and O–H stretches [10,27]. In addition, the composition and the chemical states of Ag/2D-C₃N₄/CNTs composite were determined via XPS measurements. As shown in Fig. S3a, the composite is composed of C, N, Ag and O, but the contents of Ag and O are very low. That's because only ~2 wt% of Ag was added in composite during preparation process. Trace amount of O can be chemisorbed oxygen and or introduced during calcining process. The high-resolution Ag 3d XPS spectrum shows Ag 3d_{5/2} at ~368.2 and Ag 3d_{3/2} at 374.3 eV with a ~6.1 eV energy separation, which is a characteristic property of zero valence Ag⁰ (Fig. S3b) [32,33]. The O 1s XPS spectrum show four deconvoluted peaks at ~534.2, 533.2, 532.2 and 531.3 eV attributed to O₂, C=O, H₂O and N–C=O, respectively (Fig. S3c) [10]. For C 1s XPS spectrum, the peaks core at ~288.4, 288.2, 286.61 and 284.9 eV belong to C–O, C–N–C, C–NH₂ and C=C/C=C, respectively (Fig. S3d) [10,23]. The high-resolution N 1s spectrum has three peaks at ~401.0, 399.3 and 398.7 eV, which can be attributed to C–N–H, N–(C)₃ and C–N–C, respectively, as in a typical C₃N₄ structure (Fig. S3e) [31].

Fig. 4 shows the UV-vis diffuse reflectance spectroscopy (DRS) characterization of the optical property of the photocatalysts. The bandgap of the bulk g-C₃N₄ is estimated to be ~2.74 eV from the UV-vis DRS spectrum (Fig. S4). When CNTs was introduced to the bulk g-C₃N₄, the absorption of CNTs/g-C₃N₄ was strengthened within the whole visible light region. Compared to the CNTs/g-C₃N₄, the absorption edge of CNTs/2D-C₃N₄ shifts bluely due to the well-known quantum confinement effect shifting the CB and VB in opposite directions [10,23,25,28,29]. For the Ag/2D-C₃N₄/CNTs, a peak at ~450 nm emerges due to the surface plasmon band of the supported Ag nanocubes as evidenced by the strong peak at the same wavelength for pure Ag nanocubes suspension (Fig. S5) [34,35].

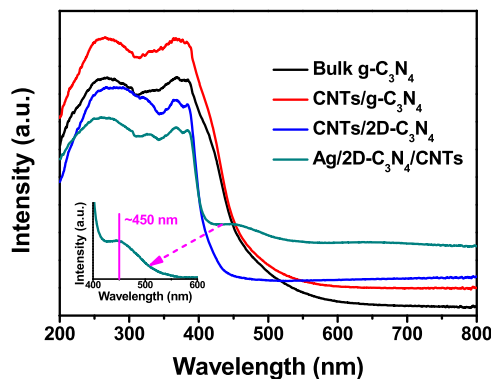


Fig. 4. UV-vis diffuse reflectance spectra of the bulk g-C₃N₄, CNTs/g-C₃N₄, CNTs/2D-C₃N₄ and Ag/2D-C₃N₄/CNTs.

To investigate the electron transport direction, the photocurrents of CNT/2D-C₃N₄ and Ag/2D-C₃N₄/CNTs under UV light irradiation ($\lambda = \sim 365$ nm) were collected. From Fig. 5a, it can be found that the blank ITO and Ag nanocubes almost did not give no clear photocurrent response. Obviously, the UV light ($\lambda = \sim 365$ nm) irradiation only excites 2D-C₃N₄ but excludes the plasmonic effect of Ag. The photocurrent of Ag/2D-C₃N₄/CNTs was not increased compared with that of CNTs/2D-C₃N₄ under UV light irradiation, indicating that the electrons at CB of 2D-C₃N₄ are not effectively trapped by Ag (Fig. 5a). Obviously, the Schottky barrier didn't form between Ag and 2D-C₃N₄. The slightly decrease in photocurrent of Ag/2D-C₃N₄/CNTs results from the slight decrease of the 2D-C₃N₄ loading in the photoelectrode because of addition of 2% Ag in composite. Thus, it can be inferred when Ag/2D-C₃N₄/CNTs is excited under the visible light irradiation, the electrons at CB of 2D-C₃N₄ can't be trapped by Ag nanocubes, but the hot electrons from the plasma effect of Ag can be injected into CB of 2D-C₃N₄, as schemed

in Fig. 5b. For the plasmonic Ag, the n-Type semiconductors are usually used to trap its plasmonic hot electron [41,42]. Good alignment of the Fermi level of Ag with band with n-Type semiconducting 2D-C₃N₄ is significant to favour efficient hot electron injection [41]. This is because the hot electrons with the high energies (φ_{HE}) can overcome the Schottky barrier (φ_{SB}) between of Ag and 2D-C₃N₄, and can be injected into CB of the neighbouring 2D-C₃N₄ [41,42], as shown in Fig. S6. Thus, the hot electrons can flow to CB of 2D-C₃N₄, and then to CNTs.

To further understand the photophysical behavior of photoexcited charge carriers, the fluorescence decay curves of the samples were measured under UV light at 337 nm. The employment of photoluminescence (PL) lifetime intends to explore the e-h recombination of the semiconductors. From the decay curves, PL intensities of all samples deviate from the exponential decay (Fig. 5c). The PL radiative lifetime is extracted by the multi-exponential fitting. Compared with the pure bulk g-C₃N₄ (3.25 ns), the PL lifetime of CNTs/g-C₃N₄ (3.37 ns) shows a slight increase because of the function of CNTs as the power pump of the electrons withdrawing the electron from CB of g-C₃N₄ and improving the e-h separation efficiency. Moreover, the PL lifetime of CNTs/2D-C₃N₄ (4.11 ns) is obviously enhanced compared with those of the bulk g-C₃N₄ and CNTs/g-C₃N₄, indicating the suppression of e-h recombination with the advantage of the 2D structure. The radiative lifetime of Ag/2D-C₃N₄/CNTs (4.09 ns) under UV light irradiation ($\lambda = 337$ nm) can not be increased compared with that of CNTs/2D-C₃N₄ because the electrons at CB of 2D-C₃N₄ can't be trapped by Ag via Schottky junction, consistent with the photocurrent results under UV light irradiation.

The introduction of CNTs can improve e-h separation of the photocatalyst. We hypothesize the hot electrons from the plasmonic effect of Ag can efficiently and unidirectionally flow to the CB of the semiconducting photocatalyst and merge with the photoexcited electrons there, and finally transport to CNTs. To

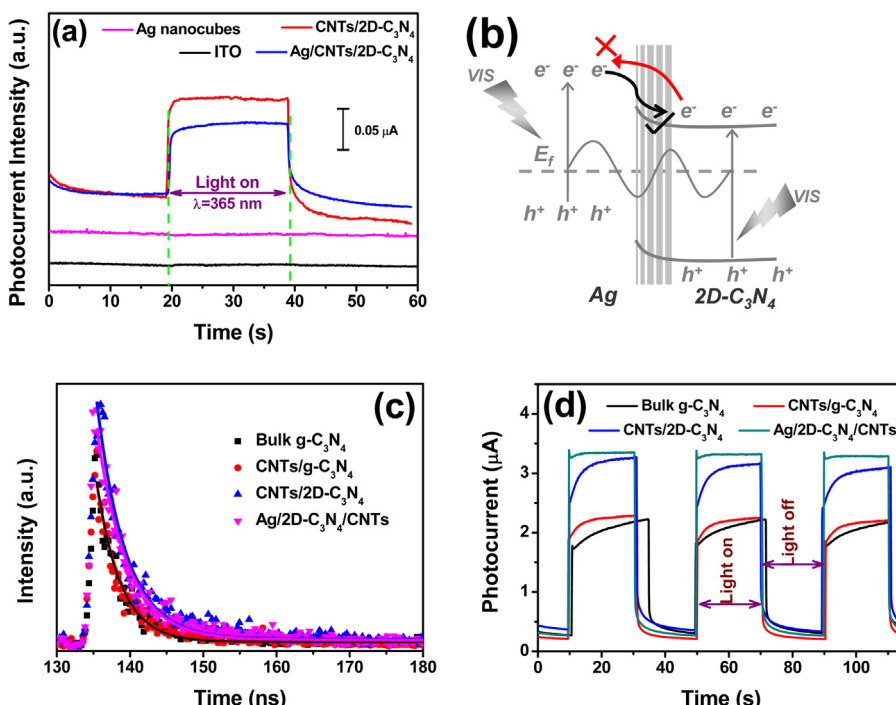


Fig. 5. (a) Photocurrent-time dependence under UV light irradiation ($\lambda = 365$ nm) of the blank ITO, Ag nanocubes, CNTs/2D-C₃N₄ and Ag/2D-C₃N₄/CNTs. The electrodes irradiated by UV light was prepared by the following method. 20 μ L of the suspension (5 mg/mL) was drop-cast onto an ITO-coated glass with a fixed area of 1 cm² (1 cm \times 1 cm), and dried under an infrared lamp. (b) Schematic illustration of the electron transfer propensities at Ag/2D-C₃N₄ interface under visible light irradiation. (c) Time-resolved fluorescence excited by the incident light of 337 nm at room temperature of the bulk g-C₃N₄, CNTs/g-C₃N₄, CNTs/2D-C₃N₄ and Ag/2D-C₃N₄/CNTs. (d) Photocurrent-time dependence under visible light irradiation of the bulk g-C₃N₄, CNTs/g-C₃N₄, CNTs/2D-C₃N₄ and Ag/2D-C₃N₄/CNTs.

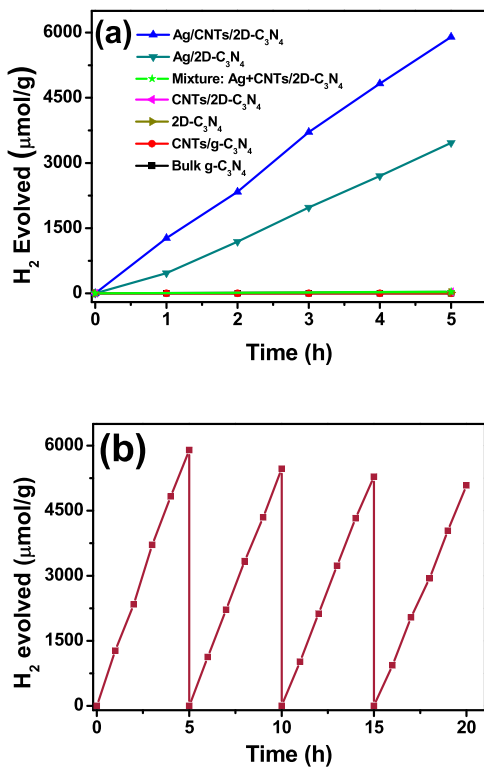


Fig. 6. (a) Photocatalytic H₂ evolution from water with the bulk g-C₃N₄, CNTs/g-C₃N₄, 2D-C₃N₄, CNTs/2D-C₃N₄, the mixture of Ag nanocubes and CNTs/2D-C₃N₄, Ag/2D-C₃N₄ and Ag/2D-C₃N₄/CNTs under visible light irradiation. (b) Stability test of Ag/2D-C₃N₄/CNTs for H₂ evolution under visible light irradiation.

verify the hypothesis, we measured the photocurrent under the visible light irradiation, as shown in Fig. 5d. The photocurrents gradually increase in the order: the bulk g-C₃N₄ < CNTs/g-C₃N₄ < CNTs/2D-C₃N₄ < Ag/2D-C₃N₄/CNTs. This result shows that the e-h recombination is effectively suppressed with the introduction of CNTs as expected. Moreover, 2D structure contributes to the e-h separation. The decoration of Ag nanocubes improves the density of the electrons at CB of the semiconductor and subsequently leads to the highest photocurrent.

The photocatalytic activities towards H₂ evolution from water splitting were finally evaluated. The Ag/2D-C₃N₄/CNTs exhibits the highest photocatalytic activity for H₂ evolution among these samples. The photocatalytic activity towards H₂ evolution for 2D-C₃N₄ can reach a kinetic rate of ~4.5 μmol/(g h). After an incorporation of CNTs as an electron pump, the CNTs/2D-C₃N₄ increase the production rate of H₂ evolution to ~7.6 μmol/(g h). With the inclusion of Ag nanocubes to form Ag/2D-C₃N₄ composite, the production rate of H₂ increases dramatically to ~693.0 μmol/(g h), suggesting the plasmonic Ag induced enhanced density of electrons participating in reduction reaction. The photocatalytic activity of Ag/2D-C₃N₄ is higher than that of CNTs/2D-C₃N₄, indicating the important role of density of electrons playing in determining the photocatalytic performance. Taking the advantage of the specific function that Ag nanocubes and CNTs play in the photocatalyst assembly, the designed Ag/2D-C₃N₄/CNTs composite photocatalyst achieves the highest H₂ evolution rate of ~1179.6 μmol/(g h) among all the tested samples (Figs. 6a, S8 and Table S1). In addition, the photocatalytic activity towards H₂ evolution of the mixture of Ag nanocubes and CNTs/2D-C₃N₄ was also carried out. The photocatalytic activity of the mixture (~8.0 μmol/(g h)) is almost the same with that of CNTs/2D-C₃N₄ (~7.6 μmol/(g h)). The photocatalytic activity towards H₂ evolution of Ag/2D-C₃N₄/CNTs composite has essential difference with that of the mixture of

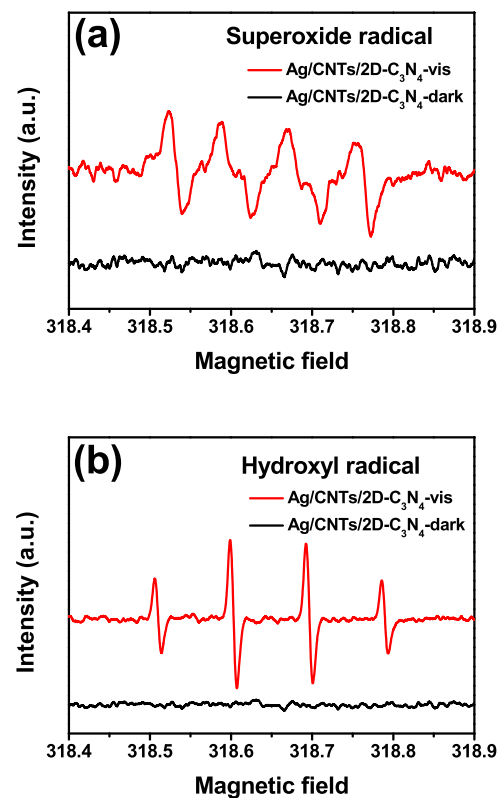


Fig. 7. ESR spectra of DMPO-O₂^{•-} (a) and DMPO•OH (b) adducts in Ag/2D-C₃N₄/CNTs aqueous dispersion systems under visible light irradiation or dark.

Ag nanocubes and CNTs/2D-C₃N₄. Additionally, the photocatalytic activity towards H₂ evolution of the mixture of Ag nanocubes and 2D-C₃N₄ (~5.5 μmol/(g h)) is also lower than that of Ag/2D-C₃N₄ composite, as shown in Table S1. These experiments also supported the proof of Ag/2D-C₃N₄/CNTs composite structure. The Ag/2D-C₃N₄/CNTs also shows an improved photocatalytic activity over other reported C₃N₄-based catalysts (Table S2), demonstrating the success of our strategy to design advanced photocatalysts. After 4 cycles, the H₂ evolution rate of Ag/2D-C₃N₄/CNTs still maintains (Fig. 6b). For the bulk g-C₃N₄ and CNTs/g-C₃N₄ samples, there is no detectable product after 5 h running (Fig. 6a), which is caused by the low redox ability and high e-h recombination rate. In addition, under visible light irradiation, the photodegradation activities of Rhodamine B (RhB) with prepared samples were shown in Fig. S9.

To study the reaction mechanism, the free radicals of the Ag/2D-C₃N₄/CNTs in aqueous solution were detected by the electron spin resonance (ESR), as shown in Fig. 7. According to the previous reports [22,25,36,37,39,43], neither bulk g-C₃N₄ nor 2D-C₃N₄ owns holes at VB capable of oxidizing H₂O/OH⁻ into •OH due to insufficiently positive potential of their VBs (Fig. S10). Thus, the holes can only oxidize the hole sacrificial reagents in water splitting or directly oxidize pollutants for the photocatalytic degradation reaction. The electrons at CB can reduce H⁺ to H₂ for H₂ evolution, and also are able to reduce O₂ to form O₂^{•-} followed by further reduction to form •OH with successive electrons and H⁺ (O₂ + e⁻ → O₂^{•-}, O₂^{•-} + e⁻ + 2H⁺ → H₂O₂, H₂O₂ + e⁻ → •OH + OH⁻) [36–40]. Our ESR clearly detected the reactions of DMPO-O₂^{•-} and DMPO•OH supporting the reaction mechanism.

4. Conclusion

In this work, we developed a design strategy for active photocatalysts for H₂ evolution under visible light irradiation. Using

2D-C₃N₄ as a base semiconductor, we introduced Ag nanocubes to induce the hot electrons from the surface plasmonic effect along with CNTs as an electron pump. In such a Ag/2D-C₃N₄/CNTs photocatalyst assembly, the hot electrons from the surface plasmonic effect of Ag merge with photoexcited ones from semiconducting 2D-C₃N₄. And the charge carrier generation in 2D-C₃N₄ can also be improved by the local electromagnetic fields of surface plasmonic Ag. Then, the electrons are steered unidirectionally to flow to the surface of CNTs. CNTs not only act as the delivery channels, but also provide extra active sites. The photocatalytic performance can be further improved with an optimized interfaces between Ag and 2D-C₃N₄ as well as CNTs and 2D-C₃N₄.

Acknowledgments

The authors genuinely appreciate the financial support of this work by the National Nature Science Foundation of China (21476097), Six talent peaks project in Jiangsu Province (2014-JNHB-014) and the Doctoral Innovation Fund of Jiangsu (KYZZ16_0339).

Appendix A. Supplementary data

Supplementary data associated with this article can be found, in the online version, at <http://dx.doi.org/10.1016/j.apcatb.2016.09.013>.

References

- [1] S. Bai, J. Jiang, Q. Zhang, Y.J. Xiong, Chem. Soc. Rev. 44 (2015) 2893–2939.
- [2] A.L. Linsebigler, G.Q. Lu, J.T. Yates, Chem. Rev. 95 (1995) 735–758.
- [3] J. Schneider, M. Matsuo, M. Takeuchi, J.L. Zhang, Y. Horiuchi, M. Anpo, D.W. Bahnemann, Chem. Rev. 114 (2014) 9919–9986.
- [4] S. Bai, L.M. Wang, X.Y. Chen, J.T. Du, Y.J. Xiong, Nano Res. 8 (2015) 175–183.
- [5] S. Bai, X.Y. Li, Q. Kong, R. Long, C.M. Wang, J. Jiang, Y.J. Xiong, Adv. Mater. 27 (2015) 3444–3452.
- [6] S. Bai, J. Ge, L.L. Wang, M. Gong, M.S. Deng, Q. Kong, L. Song, J. Jiang, Q. Zhang, Y. Luo, Y. Xie, Y.J. Xiong, Adv. Mater. 26 (2014) 5689–5695.
- [7] A.N. Cao, Z. Liu, S.S. Chu, M.H. Wu, Z.M. Ye, Z.W. Cai, Y.L. Chang, S.F. Wang, Q.H. Gong, Y.F. Liu, Adv. Mater. 22 (2010) 103–106.
- [8] C.G. Silva, J.L. Faria, Appl. Catal. B: Environ. 101 (2010) 81–89.
- [9] G.W. Yang, G.Y. Gao, C. Wang, C.L. Xu, H.L. Li, Carbon 46 (2008) 747–752.
- [10] X.J. She, L. Liu, H.Y. Ji, Z. Mo, Y.P. Li, L.Y. Huang, D.L. Du, H. Xu, H.M. Li, Appl. Catal. B: Environ. 187 (2016) 144–153.
- [11] J. Xu, X.J. Cao, Chem. Eng. J. 260 (2015) 642–648.
- [12] A. Kudo, Y. Miseki, Chem. Soc. Rev. 38 (2009) 253–278.
- [13] X.N. Guo, C.H. Hao, G.Q. Jin, H.Y. Zhu, X.Y. Guo, Angew. Chem. Int. Ed. 53 (2014) 1973–1977.
- [14] S. Linic, P. Christopher, D.B. Ingram, Nat. Mater. 10 (2011) 911–921.
- [15] J.T. Li, S.K. Cushing, P. Zheng, T. Senty, F.K. Meng, A.D. Bristow, A. Manivannan, N.Q. Wu, J. Am. Chem. Soc. 136 (2014) 8438–8449.
- [16] Z.F. Bian, T. Tachikawa, P. Zhang, M. Fujitsuka, T. Majima, J. Am. Chem. Soc. 136 (2014) 458–465.
- [17] A.O. Govorov, H. Zhang, Y.K.J. Gun'ko, Phys. Chem. C 117 (2013) 16616–16631.
- [18] X.J. She, H. Xu, Y.G. Xu, J. Yan, J.X. Xia, L. Xu, Y.H. Song, Y. Jiang, Q. Zhang, H.M. Li, J. Mater. Chem. A 2 (2014) 2563–2570.
- [19] Y. Wang, X.C. Wang, M. Antonietti, Angew. Chem. Int. Ed. 51 (2012) 68–89.
- [20] X.C. Wang, K. Maeda, A. Thomas, K. Takanabe, G. Xin, J.M. Carlsson, K. Domen, M. Antonietti, Nat. Mater. 8 (2009) 76–80.
- [21] Y. Ma, X.L. Wang, Y.S. Jia, X.B. Chen, H.X. Han, C. Li, Chem. Rev. 114 (2014) 9987–10043.
- [22] X.B. Li, G. Hartley, A.J. Ward, P.A. Young, A.F. Masters, T. Maschmeyer, J. Phys. Chem. C 119 (2015) 14938–14946.
- [23] J.H. Li, B.A. Shen, Z.H. Hong, B.Z. Lin, B.F. Gao, Y.L. Chen, Chem. Commun. 48 (2012) 12017–12019.
- [24] H.J. Kong, D.H. Won, J. Kim, S.I. Woo, Chem. Mater. 28 (2016) 1318–1324.
- [25] X.D. Zhang, X. Xie, H. Wang, J.J. Zhang, B.C. Pan, Y. Xie, J. Am. Chem. Soc. 135 (2013) 18–21.
- [26] N.Y. Cheng, J.Q. Tian, Q. Liu, C.J. Ge, A.H. Qusti, A.M. Asiri, A.O. Al-Youbi, X.P. Sun, ACS Appl. Mater. Interfaces 5 (2013) 6815–6819.
- [27] X.J. She, H. Xu, H.F. Wang, J.X. Xia, Y.H. Song, J. Yan, Y.G. Xu, Q. Zhang, D.L. Du, H.M. Li, Dalton Trans. 44 (2015) 7021–7031.
- [28] P. Niu, L.L. Zhang, G. Liu, H.M. Cheng, Adv. Funct. Mater. 22 (2012) 4763–4770.
- [29] S.B. Yang, Y.J. Gong, J.S. Zhang, L. Zhan, LL. Ma, Z.Y. Fang, R. Vajtai, X.C. Wang, P.M. Ajayan, Adv. Mater. 25 (2013) 2452–2456.
- [30] J.J. Wu, R.M. Yadav, M.J. Liu, P.P. Sharma, C.S. Tiwary, L.L. Ma, X.L. Zou, X.D. Zhou, B.I. Yakobson, J. Lou, P.M. Ajayan, ACS Nano 9 (2015) 5364–5371.
- [31] H. Xu, J. Yan, X.J. She, L. Xu, J.X. Xia, Y.G. Xu, Y.H. Song, L.Y. Huang, H.M. Li, Nanoscale 6 (2014) 1406–1415.
- [32] L. Ge, C.C. Han, J. Liu, Y.F. Li, Appl. Catal. A 409 (2011) 215–222.
- [33] L. Ge, M.X. Xu, H.B.J. Fang, Mol. Catal. A: Chem. 258 (2006) 68–76.
- [34] B. Li, R. Long, X.L. Zhong, Y. Bai, Z.J. Zhu, X. Zhang, M. Zhi, J.W. He, C.M. Wang, Z.Y. Li, Y.J. Xiong, Small 8 (2012) 1710–1716.
- [35] Q.A. Zhang, W.Y. Li, L.P. Wen, J.Y. Chen, Y.N. Xia, Chem. Eur. J. 16 (2010) 10234–10239.
- [36] F. Dong, Z.Y. Wang, Y.H. Li, W.K. Ho, S.C. Lee, Environ. Sci. Technol. 48 (2014) 10345–10353.
- [37] Z.Y. Wang, W. Guan, Y.J. Sun, F. Dong, Y. Zhou, W.K. Ho, Nanoscale 7 (2015) 2471–2479.
- [38] M.R. Hoffmann, S.T.g. Martin, W.Y. Choi, D.W. Bahnemann, Chem. Rev. 95 (1995) 69–96.
- [39] Y.J. Cui, J.H. Huang, X.Z. Fu, X.C. Wang, Catal. Sci. Technol. 2 (2012) 1396–1402.
- [40] S.C. Yan, Z.S. Li, Z.G. Zou, Langmuir 26 (2010) 3894–3901.
- [41] C. Clavero, Nat. Photonics 8 (2014) 95–103.
- [42] S. Linic, P. Christopher, D.B. Ingram, Nat. Mater. 10 (2011) 911–921.
- [43] X.J. She, J.J. Wu, J. Zhong, H. Xu, Y.C. Yang, R. Vajtai, J. Lou, Y. Liu, D.L. Du, H.M. Li, P.M. Ajayan, Nano Energy 27 (2016) 138–146.